PCCP

PAPER

Cite this: *Phys. Chem. Chem. Phys.*, 2019, **21**, 6432

Enhanced convective dissolution due to an A + B → C reaction: control of the non-linear dynamics *via* solutal density contributions

M. Jotkar, * A. De Wit and L. Rongy

Received 14th December 2018,
Accepted 19th February 2019

DOI: 10.1039/c8cp07642a

rsc.li/pccp

Chemical reactions can have a significant impact on convective dissolution in partially miscible stratifications in porous media and are able to enhance the asymptotic flux with respect to the non-reactive case. We numerically study such reactive convective dissolution when the dissolving species A increases the density of the host phase upon dissolution and reacts with a reactant B present in the host phase to produce C by an A + B → C reaction. Upon varying the difference $\Delta R_{CB} = R_C - R_B$ between the Rayleigh numbers of the product C and the reactant B, we identify four regimes with distinct dynamics when the diffusion coefficients are the same. When $\Delta R_{CB} < 0$, the density profiles are non-monotonic and the non-linear dynamics are seen to depend on the relative values of the density at the interface and the initial density of the host phase. For $\Delta R_{CB} > 0$, the monotonic density profiles are destabilizing with respect to the non-reactive case above a certain critical value ΔR_{cr}. We analyze quantitatively the influence of varying ΔR_{CB} and the ratio $\beta = B_0/A_0$ of the initial concentration of B and the solubility of A on the asymptotic steady flux, the wavelength of the fingers and the position of the reaction front. In the context of CO_2 geological sequestration, understanding how such reactions can enhance the dissolution flux is crucial for improving the efficiency and safety of the process.

1 Introduction

CO_2 capture and sequestration (CCS) is one of the promising technologies for mitigating greenhouse gas emissions.[1] This technique involves capturing CO_2 at production sites, transporting it through pipelines and injecting it into geological storage sites such as saline aquifers. Upon injection under a cap rock, a layer of less dense CO_2 is formed over the brine. When CO_2 dissolves into this underlying brine, a buoyantly unstable stratification of denser CO_2-rich brine lying on top of the less dense resident brine forms. A fingering instability can then develop, creating denser fingers sinking towards the bottom.[2–8] The convective motion facilitates further transfer of CO_2 to the host phase and increased mixing. This enhances the dissolution flux and leads to faster storage of CO_2, which is favourable to the sequestration process and instrumental in improving its efficiency and safety.

Recently, chemical reactions have been shown to be able to affect such convective dynamics.[9–13] In particular, it has been demonstrated theoretically[14–23] and experimentally[14,15,20,21,24–26] that A + B → C type of chemical reactions can amplify or slow down convective fingering when all three species are in solution depending on their relative contribution to density. Reactions can therefore not only allow for the storage of larger amounts of CO_2 during convective dissolution because they consume CO_2 (reactive effect) but can also accelerate the development of convection (reaction-induced convective effects).[18] The two effects lead to larger dissolution fluxes of CO_2, which contributes to a faster and safer storage. Therefore understanding the impact of chemical reactions on flow dynamics and how the dissolving fluxes scale with the parameters of the problem, mainly the Rayleigh numbers measuring the contribution of each chemical species to the density, and the ratio of the initial concentration of the reactants, is of tantamount importance.

Following this motivation, we numerically study dissolution-driven convection in partially miscible phases when the dissolving species A reacts with a solute B to produce C *via* an A + B → C reaction. If all three species contribute to the density of the host solution, it is possible to control the buoyancy-driven instability by selecting the properties of the reactant B for a given A. In the present study, we focus on the case where the dissolving species A increases the density of the host solution. We consider equal diffusivities of the species to focus on the solutal effects. Our objective is to numerically quantify the relative contribution of the reactive effect and that of the reaction-induced convective effect on the dissolving flux by varying the difference

Université libre de Bruxelles (ULB), Faculté des Sciences, Nonlinear Physical Chemistry Unit, C.P. 231, 1050 Brussels, Belgium. E-mail: mjotkar@ulb.ac.be, adewit@ulb.ac.be, lrongy@ulb.ac.be

in Rayleigh numbers between the product C and the reactant B *i.e.* $\Delta R_{CB} = R_C - R_B$ and the ratio $\beta = B_0/A_0$ of the initial concentration of reactant B and solubility of A in the host phase.

It was previously shown that reactions can accelerate or decelerate the convective dynamics with respect to the non-reactive case[14,16] and that the asymptotic dissolution flux of species A increases linearly with ΔR_{CB} with a change of slope at $\Delta R_{CB} = 0$.[18] More precisely, when the product C is denser than the reactant B ($\Delta R_{CB} > 0$), the density profiles are monotonic with an increased density at the interface. If C is sufficiently denser (*i.e.* ΔR_{CB} is larger than a critical value ΔR_{cr}), convective dissolution is enhanced with a larger asymptotic flux than the non-reactive flux normalized by the reactive effect and the reaction is said to have a destabilizing effect on convection. Conversely, if reactions slow down convection such that the asymptotic flux is smaller than the normalized non-reactive flux, the reaction is said to be stabilizing. When C is less dense than B ($\Delta R_{CB} < 0$), the density profiles are non-monotonic and the reaction is always stabilizing. However, a further classification of the non-monotonic density profiles based on their morphology is missing. Additionally, several questions still need to be answered: can the stabilizing reaction-induced-convective effect for $\Delta R_{CB} < 0$ overcome the reactive effect due to consumption alone? As a consequence, will this reduce the asymptotic flux value lower than that of the non-reactive equivalent or does the reactive asymptotic flux saturate when $\Delta R_{CB} \ll 0$? How does the asymptotic flux scale with very large values of ΔR_{CB}? What is the effect of changing β on the asymptotic fluxes? In this paper, we will address all the above questions.

To this end, we vary $\Delta R_{CB} \in [-6,2]$ and identify four distinct regimes. When the product C is less dense than the reactant B ($\Delta R_{CB} < 0$), the density profiles are non-monotonic and contain a local minimum. This creates a barrier to the development of the fingering instability and stabilizes the convective dynamics in comparison to the non-reactive one. We show here that these non-monotonic density profiles can be further differentiated in a regime IA and a regime IB depending on whether the density at the interface is smaller or larger than the initial density of the host solution. The stabilizing barrier of the non-monotonic profile is strongest in regime IA, which results in the formation of regular fingers that are locally stuck in space at intermediate times before merging and reaching a new steady regime. Nevertheless, the asymptotic flux of this regime IA never drops significantly below the non-reactive one, showing that the main contributor to the flux is the reactive effect occurring due to the consumption of A. Conversely, when the product C is denser than the reactant B ($\Delta R_{CB} > 0$), the monotonic density profiles lead to rapid merging of fingers to reach a steady regime with a larger flux than in the non-reactive case. Beyond a critical ΔR_{CB}, in regime III, the reaction-induced convective effect is destabilizing in comparison to the non-reactive case. It is then possible to achieve an order of magnitude increase in the asymptotic fluxes compared to the non-reactive case and effectively increase the storage rate by increasing the difference ΔR_{CB} between the density of the product C and the reactant B and by increasing the initial concentration of the reactant B.

The article is organized as follows. In Section 2 we define the model and the numerical methods used. We classify the various regimes in Section 3 based on the convective dynamics, the temporal evolution of the dissolution flux and the wavelength of the fingers. We further distinguish the regimes with non-monotonic density profiles based on the evolution of the flux, wavelength and position of the reaction front. Next, we analyze the dissolution flux, the relevant time scales including the onset time when the instability begins to grow, the fingering pattern and the storage capacity for the various parameters considered in Section 4. Finally, the main findings and highlights of our work are presented in Section 5.

2 Problem formulation

We consider a homogeneous, isotropic, isothermal porous medium in which two partially miscible aqueous phases are initially separated by a horizontal interface. The gravitational field $\mathbf{g}$ points downwards along the vertical z' axis which is perpendicular to the horizontal x' axis. The upper phase A dissolves into the lower host phase containing a reactant B with an initial concentration B_0 to produce the reactant C by a second order A + B → C reaction. All three species contribute to the density stratification. Assuming local chemical equilibrium, the concentration of A at the interface ($z = 0$) remains constant over time, and equal to its finite solubility A_0 in the host phase. The concentrations of B and C are assumed to be small enough to not affect this solubility. The host phase extends from $x' = 0$ to $x' = L'$ in the horizontal direction and from $z' = 0$ to $z' = H'$ in the vertical direction.

To obtain the governing equations, the solute concentrations, time, spatial coordinates and velocity are normalized as:[18]

$$A = A'/A_0, \quad B = B'/A_0 \quad C = C'/A_0 \tag{1a}$$

$$t = t'/t_c, \quad z = z'/l_c, \quad \mathbf{u} = \mathbf{u}'/u_c, \tag{1b}$$

where the primes denote dimensional variables. The chemical time scale $t_c = 1/(qA_0)$ with q the kinetic constant of the reaction A + B → C, the reaction–diffusion (RD) length scale $l_c = \sqrt{D_A t_c} = \sqrt{D_A/(qA_0)}$ with D_A the diffusion coefficient of A and the velocity scale $u_c = \phi l_c/t_c = \phi\sqrt{D_A q A_0}$ with ϕ the porosity of the medium.

Since all species diffuse at the same rate, the conservation relation

$$B = \beta - C, \tag{2}$$

where $\beta = B_0/A_0$ is the ratio of the initial concentration B_0 of the reactant B to the solubility A_0, allows the number of equations to be reduced. Thus, the reaction–diffusion–convection (RDC) equations for the temporal evolution of the dimensionless solute concentrations are given as

$$\frac{\partial A}{\partial t} + (\mathbf{u}\cdot\nabla)A = \nabla^2 A - AB, \tag{3a}$$

$$\frac{\partial C}{\partial t} + (\mathbf{u}\cdot\nabla)C = \nabla^2 C + AB. \tag{3b}$$

Periodic boundary conditions are used at $x = 0$ and $x = L$, no vertical flow and no flux conditions are used for A and C at $z = H$ (bottom boundary) while at $z = 0$ (interface), no vertical flow and no flux condition is used for C along with $A = 1$. We solve the RDC eqn (3) with the initial conditions

$$A(x, z = 0, t = 0) = 1 + \varepsilon\cdot\mathrm{rand}\,(x); \quad A(x, z > 0, t = 0) = 0, \tag{4a}$$

$$C(x, z, t = 0) = 0, \tag{4b}$$

Perturbations shown in eqn (4a) are introduced in the initial concentration of A at the interface in order to trigger the instability.[27,28] $\varepsilon \ll 1$ is the amplitude of the perturbations, here chosen as 10^{-3}, and rand (x) is their modulation along x, varying randomly between -1 and 1 ("white noise").

The dimensionless equation of state for the density reads

$$\rho = (\rho' - \rho_0)/\rho_c - R_B\beta = R_A A + \Delta R_{CB} C, \tag{5}$$

where ρ' is the dimensional density of the solution, ρ_0 is the density of the solvent, and $\rho_c = \phi\mu D_A/(g\kappa l_c)$ is the density scale with κ the permeability of the porous medium and μ the viscosity of the fluid. Eqn (5) expresses that density is assumed to be linearly dependent on the concentrations of the species A, B and C.[29] The Rayleigh numbers R_i (i = A, B, C) that quantify the density contribution of species i are given as

$$R_i = \frac{\alpha_i A_0 g\kappa l_c}{\phi\nu D_A} = \frac{\alpha_i A_0 g\kappa}{\phi\nu\sqrt{D_A q A_0}}, \tag{6}$$

where $\alpha_i = \frac{1}{\rho_0}\frac{\partial\rho'}{\partial c_{i'}}$ is the solutal expansion coefficient of species i and $\nu = \mu/\rho_0$ is the kinematic viscosity of the solvent.

The difference in the contributions to the density of C and B defined as

$$\Delta R_{CB} = R_C - R_B \tag{7}$$

is the key parameter of the problem.

Eqn (3) and (5) are closed using the Darcy equation for the velocity of an incompressible flow in porous media, given as

$$\nabla p = -\mathbf{u} + \rho\mathbf{e}_z, \tag{8}$$

with p the dimensionless pressure and $\mathbf{e}_z$ the unit vector along the gravity field.

Thus, for equal diffusivities, the problem is completely determined by three parameters only: R_A, ΔR_{CB} and β. We focus on the unstable density stratification problem with $R_A = 1$ and study the effect of varying ΔR_{CB} and β.

To this end, we solve the RDC eqn (3) numerically along with eqn (5) and (8) with the given boundary and initial conditions using the YALES[30] software with the DARCY_SOLVER module. The width of the computational domain is $L = 3072$ and a height $H = 2048$ is used for most of the work unless specified otherwise for some particular destabilizing cases. The dynamics depends on the specific realization of the random noise added to the initial condition in eqn (4a). We therefore average the results over 15 different realizations for a given set of parameters (R_A, ΔR_{CB}, β) to obtain robust results. Further details on the numerics can be found in ref. 18 and 31.

3 Classification of regimes

We identify four distinct regimes as shown in Fig. 1 when varying the difference ΔR_{CB} between the contribution to the density of the product C and the reactant B. The characteristic reaction–diffusion (RD)[16] density profiles are plotted for each regime. The density at the interface is denoted by ρ_I while the initial density of the host phase is denoted by ρ_b.

When $\Delta R_{CB} \geq 0$, the density profiles are monotonic with $\rho_I > \rho_b$, similar to the non-reactive equivalent. Above a critical value of ΔR_{CB} referred to as ΔR_{cr}, which is close to 0.1 for $R_A = 1$, the contribution of C to density is sufficiently large to compensate for the consumption of both A and B. The monotonic density stratifications for $\Delta R_{CB} > \Delta R_{cr}$ (classified as regime III) are then destabilizing with respect to the non-reactive case (explained later in this section) while regime II for $0 < \Delta R_{CB} < \Delta R_{cr}$ is stabilizing.

When the product C is less dense than the reactant B ($\Delta R_{CB} < 0$), there exists a local minimum in the density profile due to the formation of C at the reaction front and the density profile is non-monotonic. Although the stabilizing non-monotonic profiles were studied previously,[18] we further differentiate here regimes IA and IB based on the amplitude of the end point values (ρ_I, ρ_b). In regime IA, the density at the interface ρ_I is smaller than or equal to the initial density of the host solution ρ_b ($\rho_I \leq \rho_b$) while in regime IB, the density at the interface is larger than or equal to the initial density of the host solution ($\rho_I > \rho_b$). At $z = 0$, we have $A = 1$ and $C = \beta$ for equal diffusivities,[17] and hence

$$\rho_I = R_A + \beta\Delta R_{CB}, \tag{9}$$

while far in the bulk, where $A = C = 0$, the initial density of the host solution is

$$\rho_b = 0. \tag{10}$$

We find that the curve for which $\rho_I = \rho_b$ is given by $\Delta R' = -R_A/\beta$. We will show that depending on whether the density at the

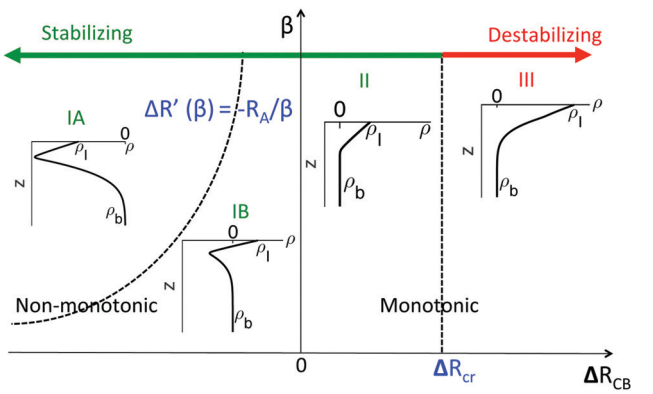

Fig. 1 Classification of the RD density profiles $\rho(z)$ in the (β, ΔR_{CB}) space: regimes IA (non-monotonic with $\rho_I \leq \rho_b$), IB (non-monotonic with $\rho_I > \rho_b$), and II (monotonic with $\rho_I > \rho_b$) are stabilizing and regime III (monotonic with $\rho_I > \rho_b$) is destabilizing. ρ_I is the density at the interface and ρ_b is the initial density of the host solution.

interface is larger or not than the initial density of the host solution *i.e.* whether the system is in regime IA ($\Delta R_{CB} < -R_A/\beta$) or IB ($0 > \Delta R_{CB} > -R_A/\beta$), a different nonlinear dynamics can be observed. We now analyze the various regimes successively.

3.1 Monotonic regimes ($\Delta R_{CB} > 0$)

Fig. 2 shows the density fields at different times for the destabilizing regime III ($\Delta R_{CB} > \Delta R_{cr}$). After a diffusive transient, the convective instability begins to grow with fingers of a given initial wavelength (Fig. 2a). Thereafter, the fingers merge rapidly reducing in number. At larger times, new fingers known as protoplumes are formed at the interface and join the older ones. Eventually, the fingers reach the bottom of the system. Species A is consumed by the reaction to produce the denser C. The fingering pattern has been shown to be mainly due to the sinking of dense C towards the bottom and by continuity, the displacement of B from the bottom towards the reaction front.[18] This implies the presence of more reactant B close to the interface to react with A which increases the dissolution flux of A. The rapid merging and birth of fingers enhances the mixing between the two phases and leads to strong convective mixing in the host phase. The process is very rapid and the system goes to shut-down as soon as the fingers reach the bottom of the solution. In order to compute the asymptotic properties, we carry out the simulations with a larger domain height *i.e.* $H = 4096$. We note that the evolution of the dynamics is similar to that of the non-reactive case[3] although on a faster time scale.

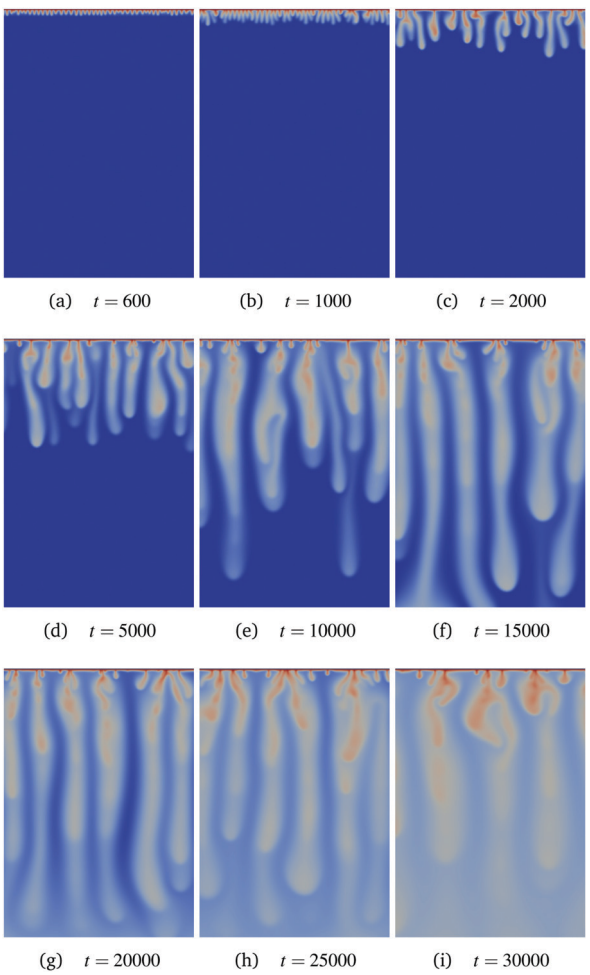

Fig. 2 Destabilizing regime III: density field at different dimensionless times t for $\Delta R_{CB} = 1.5$, $\beta = 1$ and $R_A = 1$ for height $H = 4096$. The scale varies between 0 (blue) and 2.5 (red).

To quantify the storage rate of species A in the host solution, we compute the dissolution flux J as

$$J = -\frac{1}{L}\int_0^L \left.\frac{\partial A}{\partial z}\right|_{z=0} \mathrm{d}x, \tag{11}$$

while the power-averaged mean wavelength $\bar{\lambda}$ is computed as

$$\bar{\lambda} = \left(\frac{\int_{1/L}^{1/(2\mathrm{d}x)} N|\mathscr{F}(\bar{\rho})|^2 \mathrm{d}N}{\int_{1/L}^{1/(2\mathrm{d}x)} |\mathscr{F}(\bar{\rho})|^2 \mathrm{d}N}\right)^{-1}, \tag{12}$$

where $N = 1/\lambda$ is the inverse of the wavelength and $\mathscr{F}(\bar{\rho})$ is the Fourier transform of the vertically-averaged density profile $\bar{\rho}(x,t) = \frac{1}{H}\int_0^H \rho(x,z,t)\mathrm{d}z$.

The spatio-temporal dynamics for this case can be visualized in Fig. 3 in terms of the space–time plot of the density computed at location $z = 64$ below the interface along with the temporal evolution of the corresponding flux J and the mean wavelength $\bar{\lambda}$. The rapid growth of the fingering instability and merging or birth of fingers can be seen in the space–time plot. The evolution of J suggests that the flux deviates rapidly away from the diffusive curve as the instability grows and features two peaks before reaching an asymptotic value J_{RDC}^*. The asymptotic fluxes J_{RDC}^* are larger than the non-reactive one J_{NR}^*. The two main contributions to the dissolution fluxes are the reactive effect due to consumption of A and the reaction-induced convective effect when convection is enhanced by the reaction. The reactive effect can be measured by the quantity $(1+\beta)$ corresponding to J_{RD}/J_D, the ratio between the reactive–diffusive flux and the diffusive one. We wish to quantify the contribution of the reaction-induced convective effect by comparing J_{RDC}^* to the non-reactive case coupled with the reactive effect $(1+\beta)J_{NR}^*$, referred to as the scaled non-reactive case for the sake of simplicity. We find that above a certain critical ΔR_{CB}, which is independent of β and close to 0.1 for $R_A = 1$, the convective effect is destabilizing in regime III with respect to the scaled non-reactive case *i.e.* leads to a larger asymptotic flux ($J_{RDC}^* > (1+\beta)J_{NR}^*$). This confirms the findings of previous linear stability analyses[14,16] and numerical studies.[18] In regime II, the convective effect is relatively weak and the dissolution flux increase is mainly due to the reactive effect. For example, we compare the evolution of J for regimes II ($\Delta R_{CB} = 0.1$) and III ($\Delta R_{CB} = 1.5$) in Fig. 3. Regimes II and III are qualitatively similar to all other aspects. Lastly, we see that the mean wavelength grows with time up to the shut-down limit. Large fluctuations in the values of $\bar{\lambda}$ may be attributed to the strong convective mixing and formation of protoplumes.

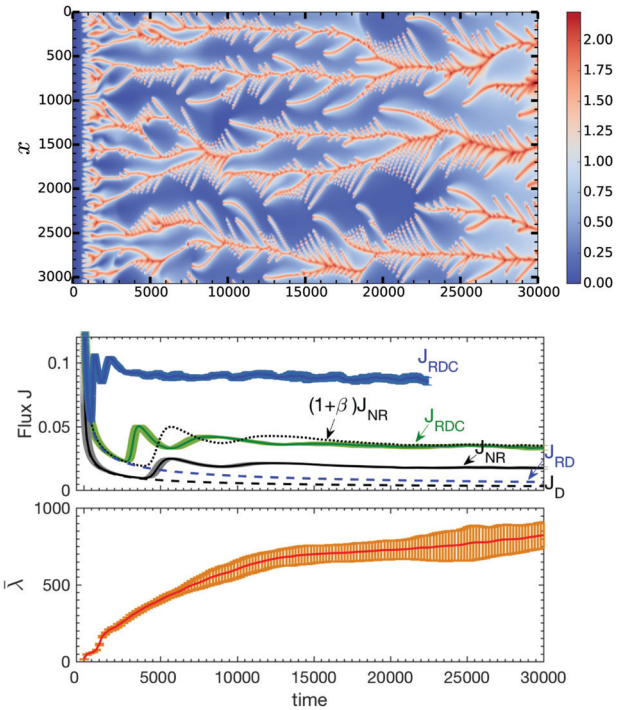

Fig. 3 Characteristics of the regime III shown in Fig. 2. Top: Space-time plot of density for ΔR_{CB} = 1.5 at z = 64 below the interface showing the onset of the instability at early times and rapid merging and birth of new fingers thereafter. Middle: Temporal evolution of the flux J showing the diffusive flux $J_D = 1/\sqrt{\pi t}$, the reactive–diffusive flux $J_{RD} = (1+\beta)/\sqrt{\pi t}$, the non-reactive flux[5] J_{NR}, the scaled non-reactive flux $(1+\beta)J_{NR}$ and the reaction–diffusion–convection flux J_{RDC} for ΔR_{CB} = 0.1 (green, regime II) and 1.5 (blue, regime III). In regime III, J_{RDC}* is significantly larger than $(1+\beta)J_{NR}$* and increases with ΔR_{CB}. Bottom: Temporal evolution of the power-averaged mean wavelength $\bar{\lambda}$ for ΔR_{CB} = 1.5.

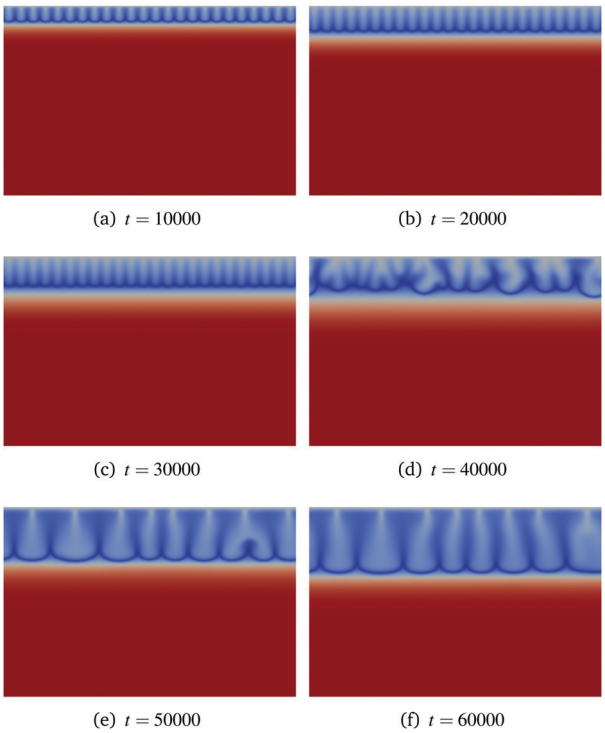

Fig. 4 Stabilizing regime IA: density field at different dimensionless times t for $\Delta R_{CB} = -2$, β = 1 and R_A = 1. The scale varies between −2 (blue) and 0 (red).

3.2 Non-monotonic regimes ($\Delta R_{CB} < 0$)

Fig. 4 shows the density field at different times for regime IA for which the density profile is non-monotonic with $\rho_I < \rho_b$. The fingers formed at the interface experience therefore a strong stabilizing barrier extending from the minimum in the density downwards. The convective dynamics in this regime is typically very slow. Once the instability begins to grow the regular fingers move away from the interface and are locally 'stuck' due to the barrier created by the larger density in the lower bulk (Fig. 4a–c). The initial number of fingers is 24 which corresponds to a wavelength ∼128. Beyond a certain time, referred to as the merging time t_{merg}, the fingers merge to give rise to a new increased wavelength stabilized by the density barrier (Fig. 4e and f). For this particular case with $\Delta R_{CB} = -2$, t_{merg} is equal to 38 600. The number of fingers after merging is equal to 8, which corresponds to a wavelength of ∼384. This merging with different constant wavelengths before and after merging is characteristic of regime IA. To illustrate this behaviour we show the spatio-temporal dynamics in Fig. 5. The space–time plot of density shows the formation of regular fingers that remain undisturbed until t_{merg} after which they merge to reach a new steady regime. Initially, the flux J follows the diffusive one J_{RD}. Following the onset of the instability where the regular fingers are formed, a peak in the value of J is observed. Thereafter, the flux scales as $J \sim t^{-1/2}$ at intermediate times where the locally 'stuck' fingers are observed. After t_{merg}, a second step increase in J is seen, followed by the steady flux J_{RDC}*. Meanwhile, after the onset of the instability, a constant value of the power-averaged mean wavelength $\bar{\lambda}$ is observed until t_{merg} where a step increase occurs leading to a new larger value.

In regime IA with $\rho_I \leq \rho_b$, the regular fingers formed are locally 'stuck' due to the stabilizing barrier created by the local minimum in the density profiles. This constrains the wavelength of the fingers formed and decreasing ΔR_{CB} further increases the amplitude of the local minimum and hence the strength of the barrier. This implies that the regular locally 'stuck' fingers exist for longer transients before merging.

Fig. 6 shows the density fields at different times for regime IB, for which the density profile is still monotonic but $\rho_I > \rho_b$. Characteristics of regime IA including merging of fingers at t_{merg} and a constant number of fingers before and after merging are seen here too. However, because here $\rho_I > \rho_b$, the stabilizing barrier is not strong enough to block the convective dissolution strength at the interface. The dynamics are then typically faster than in regime IA and transitions between regimes are smoother. For $\Delta R_{CB} = -0.5$, the number of fingers before merging is equal to 30 (Fig. 6a and b) which is larger than in regime IA. The equivalent wavelength is ∼102. The merging occurs at much shorter times compared to regime IA and is much less abrupt. The uniform number of fingers after merging is equal to 12 for this case (Fig. 6f) with equivalent wavelength ∼256. The number of fingers formed

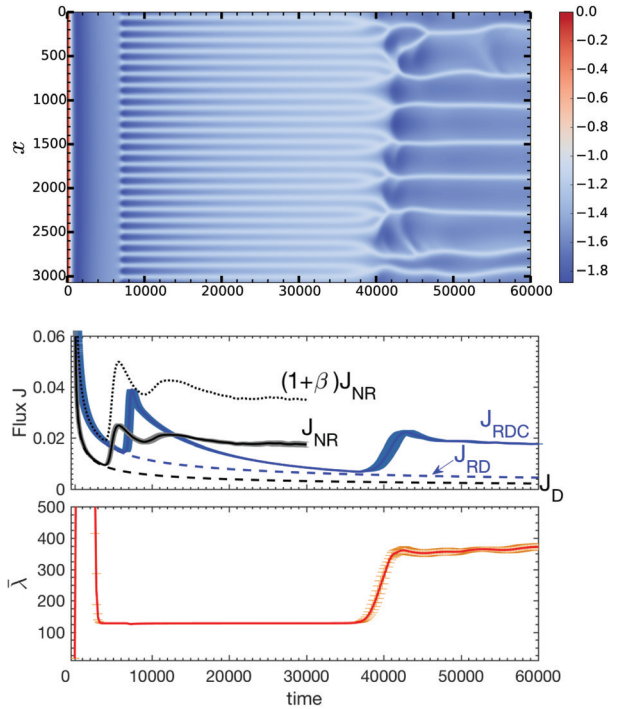

Fig. 5 Characteristics of regime IA shown in Fig. 4. Top: Space–time plot of density showing the formation of regular fingers after the onset of the instability that remain locally stuck up to $t_{merg} \sim 40\,000$ and merge afterwards to reach a new steady regime. Middle: Temporal evolution of the reactive flux J_{RDC} (in blue) showing that initially the flux follows $J_{RD} = (1+\beta)/\sqrt{\pi t}$, followed by an increase close to the onset of the instability, a scaling $J \sim 1/\sqrt{t}$ at intermediate times up to a second step at t_{merg} to reach a steady value. Bottom: Power-averaged mean wavelength $\bar{\lambda}$ showing the intermediate uniform wavelength that increases after t_{merg}.

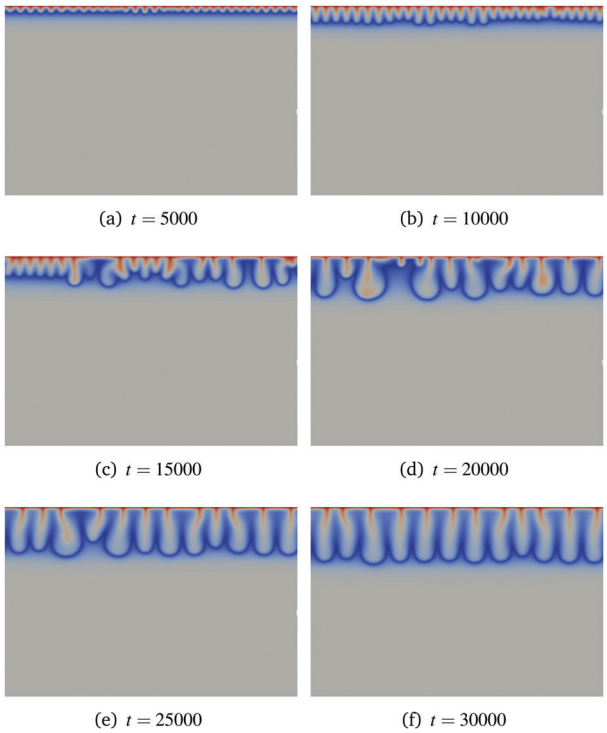

Fig. 6 Stabilizing regime IB: density field at different dimensionless times t for $\Delta R_{CB} = -0.5$, $\beta = 1$ and $R_A = 1$. The scale varies between −0.5 (blue) and 0.5 (red).

after merging increases with ΔR_{CB} whereas, in regime IA, it is similar for all values of ΔR_{CB} as will be detailed below. Fig. 7 shows the space–time plot of density, J and $\bar{\lambda}$ for regime IB. The first peak in J close to the onset of the instability and the second step increase close to merging of fingers are seen here at shorter time scales compared to regime IA. Merging occurs less abruptly than in regime IA as can also be seen in the temporal evolution of $\bar{\lambda}$.

3.3 Comparison between regimes IA and IB

To further quantify the difference between the dynamics in regimes IA and IB, we compare the temporal evolution of the position of the reaction zone z_f, $\bar{\lambda}$ and J in Fig. 8 for various $\Delta R_{CB} < 0$.

We define the horizontally-averaged reaction rate profile $\bar{r}(z)$ as

$$\bar{r}(z,t) = \frac{1}{L}\int_0^L A(x,z,t)B(x,z,t)\mathrm{d}x, \qquad (13)$$

and next compute the position of the reaction front as the first moment of $\bar{r}(z,t)$ *i.e.*

$$z_f(t) = \frac{\int_0^H z\bar{r}(z,t)\mathrm{d}z}{\int_0^H \bar{r}(z,t)\mathrm{d}z}. \qquad (14)$$

Initially, in the diffusive regime, the reaction front moves away from the interface as $z_f \sim \sqrt{t}$. After the onset of convection, at the intermediate times where regular fingers are observed, there exists a slight jump in the values of z_f and thereafter it scales once again as $z_f \sim \sqrt{t}$ up to the merging time t_{merg}. In Fig. 8(a), t_{merg}, computed as the time at which $\bar{\lambda}$ experiences an inflection point, is denoted by the vertical dashed lines in the respective colours for the different ΔR_{CB}. After the regular fingers merge to increase the wavelength to another larger steady value, the reaction zone scales as $z_f \sim t$. However, in regime IB for $\Delta R_{CB} > -0.8$, such an intermediate scaling of $z_f \sim \sqrt{t}$ is not observed and beyond the initial diffusive behaviour, the $z_f \sim \sqrt{t}$ scaling is seen, as illustrated for $\Delta R_{CB} = -0.2$ and -0.5. It is to be noted that regime IB acts as a transition between regimes IA and II. More precisely, close to $\Delta R'$ in regime IB, characteristics similar to regime IA with intermediate fingers locally 'stuck' in space and merging to reach a new steady regime are observed. However, closer to $\Delta R_{CB} = 0$, for example for $\Delta R_{CB} = -0.2$ and -0.5 the fingers overcome the barrier created by the minimum in the density profile and in the steady regime the fingers are very irregular, similar to that seen for the monotonic density profiles in regimes II and III.

After the departure from the diffusive regime, when the instability grows, a peak in the values of $\bar{\lambda}$ is observed (see Fig. 8(b)); thereafter $\bar{\lambda}$ remains steady for intermediate times up to t_{merg}. After t_{merg} a step change in the wavelength to a higher constant value is observed for regimes IA. The values of $\bar{\lambda}$ reached

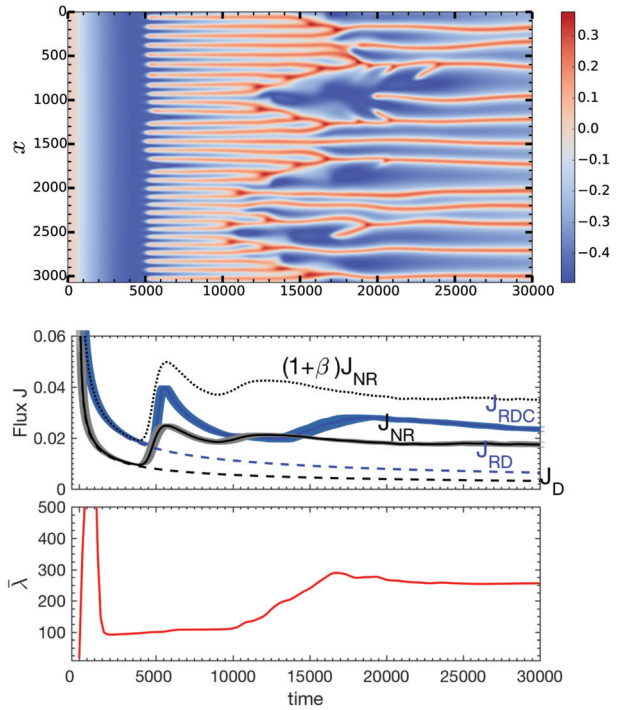

Fig. 7 Characteristics of regime IB shown in Fig. 6. Top: Space–time plot of density showing the regular fingers that merge gradually as opposed to an abrupt change seen in regime IA. Middle: Temporal evolution of the flux J showing the initial diffusive limit followed by a first peak when convection sets in and a second step increase due to merging occurring sooner than that seen for regime IA. Bottom: Power-averaged mean wavelength $\bar{\lambda}$ showing the regular fingers occurring for shorter intermediate time limit and sooner merging than in regime IA.

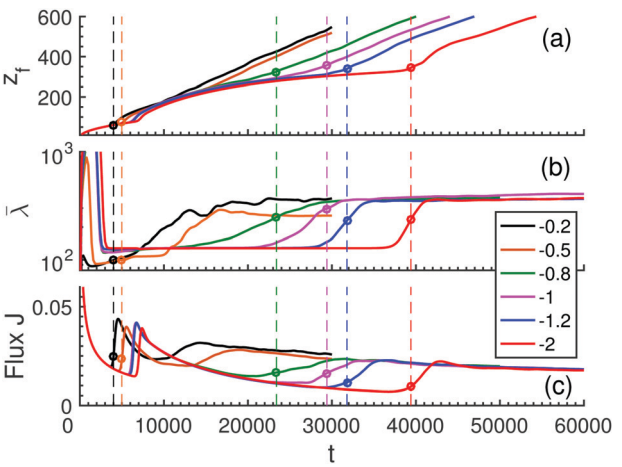

Fig. 8 Temporal evolution of the (a) reaction front position z_f, (b) power-averaged mean wavelength $\bar{\lambda}$ and (c) transient flux J for different ΔR_{CB} marked in the inset in regimes IA and IB with $\beta = 1$ and $R_A = 1$. The dashed vertical lines represent the merging time t_{merg} for the respective cases and the solid circles in the corresponding colours indicate the values at t_{merg} for the different quantities.

at asymptotic times is the same for all $\Delta R_{CB} < -R_A/\beta$ in regime IA. In contrast, in regime IB, a gradual increase from the initial wavelength to an asymptotic one is seen occurring at shorter times and the asymptotic value of $\bar{\lambda}$ is different for the different ΔR_{CB}.

Simultaneously, the transient flux scales as $t^{-1/2}$ initially in the diffusive regime before it experiences a first peak when the instability begins to grow (see Fig. 8(c)). Thereafter in regime IA, the second step increase corresponds to the merging of the fingers at t_{merg} after which a steady regime is reached. This time increases with a decrease in ΔR_{CB}. In regime IB, the occurrence of the second step increase is almost immediate after the first one and followed by a steady regime at relatively short times. Thus, the dynamics of the two regimes are distinct and dictated by the morphology of the density profiles.

To summarize this section, we have characterized the distinct convective dynamics of regimes IA, IB, II and III. Non-monotonic density profiles in regime IA with $\rho_I \leq \rho_b$ are the most stabilizing ones with typically slow dynamics, merging of fingers with uniform wavelength before and after merging, and characteristically 'stuck' fingers. Non-monotonic density profiles with $\rho_I > \rho_b$ in regime IB are less stabilizing compared to IA and reach a steady regime sooner with a wavelength after merging that depends on ΔR_{CB}. Regime II is faster than IA and IB but the asymptotic flux values are lower than $(1+\beta)J_{NR}^*$ as the product C and reactant B are almost equally dense. Beyond $\Delta R_{cr} \approx 0.1$ for $R_A = 1$ in regime III, the convective dynamics is very fast and destabilizing with an asymptotic flux larger than $(1+\beta)J_{NR}^*$.

4 Parametric study

In this section we first recall the effect of increasing ΔR_{CB} on the dissolution flux for $\beta = 1$ and next, we analyze the effect of varying β.

Fig. 9 shows the temporal evolution of the dissolution flux J in the different regimes for $\Delta R_{CB} \in [-2,1.5]$ with $\beta = 1$. As mentioned in Section 3, the dissolution flux J asymptotically fluctuates around an asymptotic value, referred to as J^*. The flux for the non-reactive case is denoted J_{NR} here along with the scaled non-reactive case $(1+\beta)J_{NR}$. We see that asymptotically all reactive cases yield $J^* > J_{NR}^*$. Chemical reactions thus always allow for a faster dissolution of more CO_2 than the

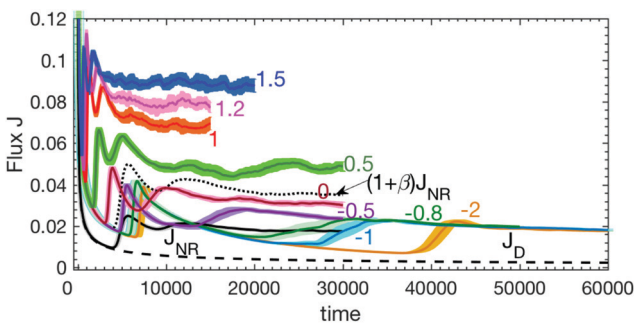

Fig. 9 Temporal evolution of the dissolution flux J of species A for different ΔR_{CB} indicated in the plot with $\beta = 1$ and $R_A = 1$. Diffusive flux J_D is denoted by the dashed black line, while the non-reactive J_{NR} and the scaled non-reactive $(1+\beta)J_{NR}$ fluxes are denoted by black solid and dotted lines, respectively.

non-reactive case. The asymptotic flux J^* can be increased by increasing ΔR_{CB} from regime IA to III. More precisely, the storage can be faster when the product C is denser than the reactant B. We note however that below $\Delta R_{CB} \approx 0.1$, in regimes IA, IB and II the J^* values are lower than the non-reactive case scaled by the reactive effect alone $(1+\beta)J_{NR}{}^*$. In these regimes, the increase of the dissolution flux is mainly due to the reactive effect occurring due to the consumption of A by the reaction. Above the critical ΔR_{cr}, convection is stronger than in the non-reactive case and hence the regime is referred to as destabilizing.

Next, we study the effect of β by analyzing the relevant time scales including the onset time for instability t_0, the non-linear time t_{NL} and the merging time t_{merg}.

We define the onset time t_0 for the onset of convection on the basis of the magnitude of velocity computed as $U^2(t) = \int_0^H \int_0^L \left[u_x^2(x,z,t) + u_z^2(x,z,t)\right] \mathrm{d}x\mathrm{d}z$. For any value of ΔR_{CB}, U^2 decreases until a given onset time t_0 when it reaches its minimum before it begins to grow as in the non-reactive case.[5] After some time, non-linearities become significantly large and the dynamics differ from a diffusive one. We define t_{NL} as the time when the relative difference between the averaged mixing length z_m (defined as the most advanced position along z where $A + C > s$, with s being a small arbitrary threshold chosen here to be 0.01) and its diffusive prediction z_m^{RD} is greater than 5%. Here $z_m^{RD}(t) = 2\sqrt{t}\,\mathrm{erf}^{-1}(1 - s/(1+\beta))$ with erf^{-1} being the inverse error function. We recall that the merging time t_{merg} for regimes IA and IB, defined as the time where the regular locally 'stuck' fingers merge to reach a new steady regime, is computed as the time at which the power-averaged mean wavelength $\bar{\lambda}$ experiences an inflection point.

Fig. 10 shows the different relevant times t_0, t_{NL} and t_{merg} (for regimes IA and IB) for different β and ΔR_{CB}. For $\Delta R_{CB} \leq 0$, all characteristic times increase with a decrease in ΔR_{CB} for a given β and this effect increases with β. To explain this behaviour, we recall that in these regimes the non-monotonic density profiles contain a local minimum which acts like a stabilizing barrier to the convective dynamics. For $\Delta R_{CB} < 0$, as $|\Delta R_{CB}|$ increases, the amplitude of the local minimum increases in magnitude and the stabilizing barrier becomes stronger. Thus, decreasing ΔR_{CB} below 0 implies a longer transient before the onset of convection, its non-linear breakdown and merging to reach a steady regime. Increasing β leads to an even larger stabilizing barrier created by the increased magnitude of the local minimum in the density profiles. Additionally, this barrier fixes the wavelength of the fingers formed as observed in the formation of regular intermediate locally 'stuck' fingers. In contrast, if $\Delta R_{CB} > 0$, the various times become substantially smaller with an increase in ΔR_{CB} for a given β and this effect increases with β. A cross-over in the values of t_{NL} and t_0 is observed close to $\Delta R_{cr} \approx 0.1$. This confirms the stabilizing effect of regimes IA, IB and II and the destabilizing effect of regime III.

To understand the fingering pattern, we also analyze the number of fingers soon after the onset of the instability $t \gtrsim t_0$ and after merging $t \gtrsim t_{merg}$ for regimes IA and IB. This is shown in Fig. 11 for different β and ΔR_{CB} (for one realization). In regime IA, the number of fingers is more or less constant irrespective of the value of β and $\Delta R_{CB} < \Delta R'$. This is due to the fact that the density barrier created by the local minimum blocks the development of the convective instability. Any decrease in the value of ΔR_{CB} only increases the strength of the stabilizing barrier but does not change the difference between the density at the interface ρ_I and the density in the minimum equal to $\beta\Delta R_{CB}$ (eqn (5) with $A = 0$ and $C = \beta$). There exists a slight difference in the formation of fingers in regime IB where an increase in ΔR_{CB} leads to an increase in the number of fingers formed after t_0 and after t_{merg}. When $\Delta R_{CB} > 0$, the number of fingers formed at the onset of the convective instability t_0 increases with ΔR_{CB} in regimes II and III. Thus, an increase in ΔR_{CB} has a destabilizing effect.

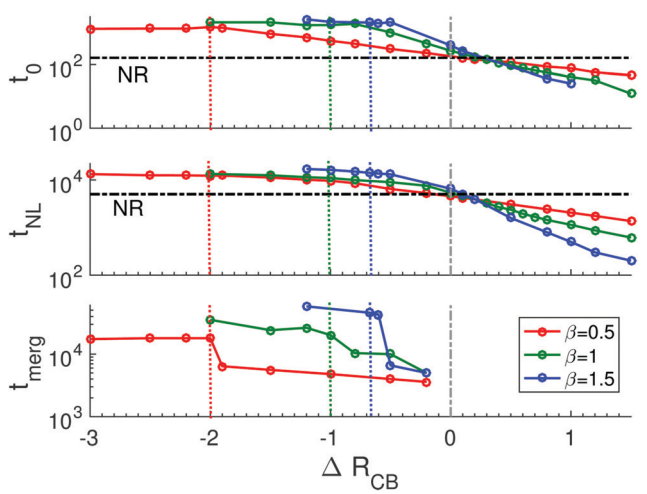

Fig. 10 Onset time t_0 (top), non-linear time t_{NL} (middle) and merging time t_{merg} (bottom for regimes IA and IB) for different values of β as a function of ΔR_{CB}. Horizontal black dashed-dotted lines correspond to the NR case while vertical grey dashed-dotted lines indicate $\Delta R_{CB} = 0$. Vertical dotted lines in different colours represent the transition from regime IA to IB *i.e.* $\Delta R' = -R_A/\beta$ for the different β and $R_A = 1$.

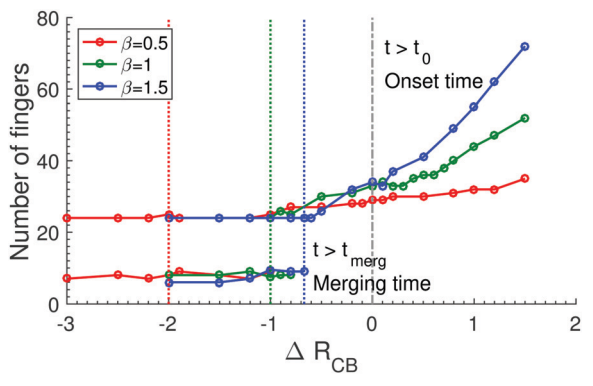

Fig. 11 Number of fingers observed in one realization soon after onset time $t \gtrsim t_0$ and after merging at steady regime $t \gtrsim t_{merg}$ for regimes IA and IB as a function of ΔR_{CB} and different β shown in the inset. The vertical lines are similar to Fig. 10.

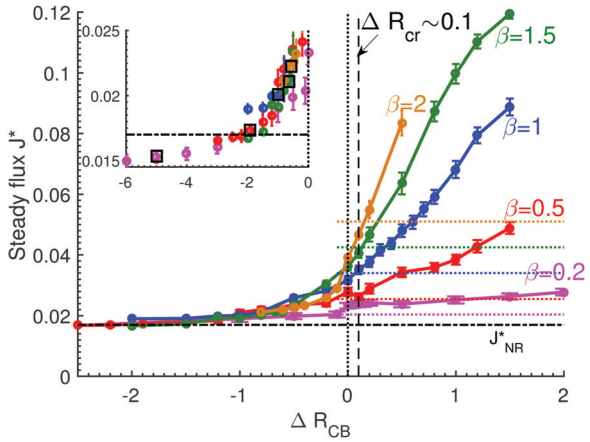

Fig. 12 Asymptotic dissolution flux J^* as a function of ΔR_{CB} for different β indicated with different colours for $R_A = 1$. The corresponding asymptotic flux for the NR case[5] J_{NR}^* is denoted by the horizontal black dashed-dotted line and that for the scaled NR, $(1 + \beta)J_{NR}^*$, is denoted by horizontal dotted lines for each β in the respective colours. Transition from regime IA to regime IB at $\Delta R' = -R_A/\beta$ is indicated by the solid black rectangles for the different β in the inset. The vertical black dashed line $\Delta R_{cr} \sim 0.1$ corresponds to the transition from II to III.

Finally, we quantify in Fig. 12 the long-time fate of A or the asymptotic dissolution flux J^* as a function of ΔR_{CB} and β to understand the coupled effect of reaction and convection. J^* is computed as the average over the last time interval >3000 when the variation of the flux with time (least-squares fitted slope) is not larger than a small threshold, here arbitrarily chosen to be 10^{-6}. Fluctuations around the values of J^* may be attributed to reinitiation where the protoplumes from the boundary layer join the older fingers.

We find that J^* increases with ΔR_{CB} for a given β and that this effect is magnified when β increases. The asymptotic flux for the non-reactive case J_{NR}^* is approximately 0.019, which is in agreement with the value in the literature.[5] We recall that the objective of the present study is to quantify the relative contribution of the consumption of A and of the reaction-induced convective effect on the storage rate of A. The reactive effect due to consumption can be quantified by multiplying the diffusive flux by a factor $(1 + \beta)$. The convective effect for a reactive system is measured by comparing J^* to the scaled non-reactive convective flux $(1 + \beta)J_{NR}^*$. As mentioned in the previous section, regimes IA, IB and II yield J^* lower than this scaled non-reactive convective flux and the convective effect is thus stabilizing with respect to the non-reactive case. Conversely, in regime III, J^* is larger than $(1 + \beta)J_{NR}^*$ and the convective effect is thus destabilizing. This effect becomes stronger with an increase in ΔR_{CB} and β. A minimum amount of ΔR_{CB}, which is approximately $\Delta R_{cr} \sim 0.1$ for all cases of β studied here, is needed to achieve accelerated convection due to reaction. Similarly, a threshold of $0.32R_A$ was predicted by the linear stability analysis[16] above which increasing ΔR_{CB} has a destabilizing effect on perturbation growth rates relative to the non-reactive case.

When C is less dense than B, an increase in β or a decrease in ΔR_{CB} has a stabilizing effect. However, in regime IA *i.e.* for $\Delta R_{CB} < \Delta R'$, any further decrease in ΔR_{CB} has a negligible effect on the convective dynamics and J^* gets saturated with $\Delta R_{CB} \ll 0$. This can be explained as follows. For equal diffusivities of all three species assumed here, we recall that the density at the interface is $\rho_I = R_A + \Delta R_{CB}\beta$, the density at the reaction front is $\Delta R_{CB}\beta$ while the initial density of the host solution is 0. For $\Delta R_{CB} < 0$ in regimes IA and IB, the RD density profiles contain a local minimum in the host solution. The difference of density at the origin of the instability is given by the difference in density between the interface and at the minimum *i.e.* at the reaction front; and is equal to R_A. Changing the values of ΔR_{CB} or β does not alter this difference but increases the amplitude of the stabilizing barrier, *i.e.* the difference of density $-\Delta R_{CB}\beta$ between the minimum and the bulk of the solution. This explains that any decrease in the values of ΔR_{CB} or β has a very mild effect on J^* in regimes IA and IB.

To summarize, the dissolution fluxes and their asymptotic values show that the convective effects in regimes IA, IB and II are stabilizing with respect to the non-reactive case whereas this effect is destabilizing in regime III. When C is denser than B, the asymptotic flux increases with β and conversely, when C is less dense than B, J^* decreases slightly with an increase in β. However, when $\Delta R_{CB} \ll 0$ the asymptotic flux saturates to a constant value which never significantly drops below the non-reactive one J_{NR}^*.

5 Conclusions

We have numerically studied the non-linear convective dynamics developing when a solute A dissolves with a finite solubility A_0 into a host solution containing B to produce C by an A + B → C type of reaction. In particular, we have studied the influence of varying (i) ΔR_{CB}, the difference in the contribution to density of the product C and reactant B, up to relatively extreme values and (ii) the ratio $\beta = B_0/A_0$ on the properties of convective dissolution. We have focused here on the case where the dissolving species A increases the density of the host solution ($R_A > 0$), *i.e.* when the non-reactive density stratification is buoyantly unstable and all species diffuse equally. While in the non-reactive case only one type of density profile can develop, two types of density profiles are possible in the reactive case: a monotonic one similar to the non-reactive case for $\Delta R_{CB} > 0$ and a non-monotonic one for $\Delta R_{CB} < 0$. We have shown here that the non-monotonic profiles can be further classified into two different regimes depending on the difference between the density at the interface and the initial density of the host solution.

We identify four regimes with distinct dynamics upon increasing ΔR_{CB}. Regime IA obtained for $\Delta R_{CB} \leq \Delta R' = -R_A/\beta$ features non-monotonic density profiles where the density at the interface is smaller than or equal to the initial density in the host solution, $\rho_I \leq \rho_b$. Dynamics in regime IA are characteristically slow with regular fingers formed after the onset of instability that remain 'stuck' locally in space due to the large stabilizing barrier created by the local minimum in the density

profile. Beyond a certain time, referred to as merging time or t_{merg}, the fingers merge to reach a new steady regime in which the wavelength of fingers is larger than at short times but constant as well. In this frozen regime, the steady flux is of the order of the one in the non-reactive case. Regime IB ($\Delta R' < \Delta R_{CB} < 0$) corresponds to non-monotonic density profiles where the density at the interface is larger than the initial density in the host solution, $\rho_I > \rho_b$. Similar to regime IA, the formation of regular fingers and their merging to reach a steady regime is also observed in regime IB, with a few distinct features. The density barrier created by the local minimum in the profiles is relatively weaker than in regime IA. As a consequence, the regular fingers formed after the onset of the instability merge (t_{merg}) at earlier times. Moreover, the number of fingers after merging is larger than in regime IA and this number increases with ΔR_{CB}. Regimes II and III with monotonic density profiles and dynamics similar but faster than the non-reactive one, occur when $\Delta R_{CB} > 0$.

After classifying the distinct dynamics, we have quantified the long-time fate of species A in terms of its storage rate. In reactive–convective dissolution, the enhanced storage rates are attributed to the reactive effect due to the consumption of A and to the reaction-induced convective effects when the reaction accelerates the development of the convective instability. We measure the convective effect on the asymptotic dissolution flux J^* for the various regimes and find that regimes IA, IB and II are stabilizing compared to the non-reactive case scaled by the reactive effect, *i.e.* $J^* < (1 + \beta)J_{NR}{}^*$, while regime III is destabilizing with $J^* > (1 + \beta)J_{NR}{}^*$ (see Fig. 12). Above a certain critical value ΔR_{cr}, which is independent of β and equal to 0.1 for $R_A = 1$, the convective effect is destabilizing and this effect increases with ΔR_{CB} and β. This suggests that it is possible to obtain larger storage rates by increasing β and $\Delta R_{CB} > \Delta R_{cr}$. The increase of β not only amplifies the consumption effect by a factor $(1 + \beta)$, but also magnifies the reaction-induced convection when the density between C and B is above a certain critical value.

Conversely, when $\Delta R_{CB} < \Delta R_{cr}$, the reaction-induced convective effect is stabilizing and this effect becomes stronger with a decrease in ΔR_{CB} and an increase in β. When C is less dense than B, the local minimum in the density profile creates a barrier decelerating the formation of the convective instability. This barrier becomes stronger when there is more reactant B present initially. However, even for extreme values $\Delta R_{CB} \ll 0$, the stabilizing convective effect does not overcome the reactive effect and the asymptotic flux gets saturated with ΔR_{CB}. More precisely, the stabilizing convective effect in regime IA, where the density profiles are such that $\rho_I \leq \rho_b$, is independent of the amplitude of the local minimum and a decrease in ΔR_{CB} only affects slightly the relevant times. The values of J^* do not drop significantly below the non-reactive one $J_{NR}{}^*$.

In the context of CO_2 sequestration, the above conclusions are essential for determining the optimal storage sites at a subsurface level to achieve enhanced convective dissolution with an objective of improving the safety and efficiency of the process. Understanding the influence of the various parameters involved in the convective dynamics is of significant importance. For other applications where it is advantageous to gain control over the convective dissolution, we demonstrate that it is possible to do so with the help of chemical reactions by selecting the appropriate reactant with the adequate initial composition.

Conflicts of interest

There are no conflicts to declare.

Acknowledgements

We thank B. Knaepen and V. Loodts for their help and support concerning the YALES2 code. We gratefully acknowledge the financial support from the ULB foundation and from the FRS-FNRS PDR CONTROL project.

Notes and references

1 Intergovernmental Panel on Climate Change (IPCC) special report on Carbon Dioxide Capture and Storage, Cambridge University Press, New York, 2005.
2 G. S. Pau, J. B. Bell, K. Pruess, A. S. Almgren, M. J. Lijewski and K. Zhang, *Adv. Water Resour.*, 2010, **33**, 443–455.
3 M. T. Elenius and K. Johannsen, *Comput. Geosci.*, 2012, **16**, 901–911.
4 A. C. Slim, M. M. Bandi, J. C. Miller and L. Mahadevan, *Phys. Fluids*, 2013, **25**, 024101.
5 A. C. Slim, *J. Fluid Mech.*, 2014, **741**, 461–491.
6 H. E. Huppert and J. A. Neufeld, *Annu. Rev. Fluid Mech.*, 2014, **46**, 255–272.
7 H. Emami-Meybodi, H. Hassanzadeh, C. P. Green and J. Ennis-King, *Int. J. Greenhouse Gas Control*, 2015, **40**, 238–266.
8 C. Thomas, S. Dehaeck and A. De Wit, *Int. J. Greenhouse Gas Control*, 2018, **72**, 105–116.
9 J. Ennis-King and L. Paterson, *Int. J. Greenhouse Gas Control*, 2007, **1**, 86–93.
10 K. Ghesmat, H. Hassanzadeh and J. Abedi, *J. Fluid Mech.*, 2011, **673**, 480–512.
11 S. S. S. Cardoso and J. T. H. Andres, *Nat. Commun.*, 2014, **5**, 5743.
12 T. J. Ward, K. A. Cliffe, O. E. Jensen and H. Power, *J. Fluid Mech.*, 2014, **747**, 316–349.
13 T. J. Ward, O. E. Jensen, H. Power and D. Riley, *J. Fluid Mech.*, 2014, **760**, 95–126.
14 V. Loodts, C. Thomas, L. Rongy and A. De Wit, *Phys. Rev. Lett.*, 2014, **113**, 114501.
15 M. A. Budroni, L. A. Riolfo, L. Lemaigre, F. Rossi, M. Rustici and A. De Wit, *J. Phys. Chem. Lett.*, 2014, **5**, 875–881.
16 V. Loodts, L. Rongy and A. De Wit, *Phys. Chem. Chem. Phys.*, 2015, **17**, 29814.
17 V. Loodts, P. M. J. Trevelyan, L. Rongy and A. De Wit, *Phys. Rev. E*, 2016, **94**, 043115.

18 V. Loodts, B. Knaepen, L. Rongy and A. De Wit, *Phys. Chem. Chem. Phys.*, 2017, **19**, 18565–18579.
19 P. Ghoshal, M. C. Kim and S. S. S. Cardoso, *Phys. Chem. Chem. Phys.*, 2017, **19**, 644–655.
20 C. Wylock, A. Rednikov, P. Colinet and B. Haut, *Chem. Eng. Sci.*, 2017, **157**, 232–246.
21 M. A. Budroni, C. Thomas and A. De Wit, *Phys. Chem. Chem. Phys.*, 2017, **19**, 7936.
22 V. Loodts, H. Saghou, B. Knaepen, L. Rongy and A. De Wit, *Fluids*, 2018, **3**, 83.
23 M. C. Kim and S. S. S. Cardoso, *Phys. Fluids*, 2018, **30**, 094102.
24 C. Wylock, A. Rednikov, B. Haut and P. Colinet, *J. Phys. Chem. B*, 2014, **118**, 11323–11329.
25 C. Thomas, V. Loodts, L. Rongy and A. De Wit, *Int. J. Greenhouse Gas Control*, 2016, **53**, 230–242.
26 I. Cherezov and S. S. S. Cardoso, *Phys. Chem. Chem. Phys.*, 2016, **18**, 23727–23736.
27 M. Bestehorn and A. Firoozabadi, *Phys. Fluids*, 2012, **24**, 114102.
28 N. Tilton, D. Daniel and A. Riaz, *Phys. Fluids*, 2013, **25**, 092107.
29 P. Cheng, M. Bestehorn and A. Firoozabadi, *Water Resour. Res.*, 2012, **48**, W09539.
30 V. Moureau, P. Domingo, L. Vervisch and A. Riaz, *C. R. Mec.*, 2011, **339**, 141–148.
31 V. Loodts, PhD thesis, Université libre de Bruxelles, 2016.

